A Density Functional Theory (DFT) and Time-Dependent Density Functional Theory (TDDFT) Study on Optical Transitions in Oligo(*p*-phenylenevinylene)−Fullerene Dyads and the Applicability to Resonant Energy Transfer

Teemu L. J. Toivonen* and Terttu I. Hukka

Institute of Materials Chemistry, Tampere University of Technology, P.O. Box 541, 33101 Tampere, Finland

Received: December 7, 2006; In Final Form: February 21, 2007

The optical transitions of three different size oligo(*p*-phenylenevinylene)−fullerene dyads (OPV_n−MPC_{60}; $n = 2-4$) and of the corresponding separate molecules are studied using density functional theory (DFT) and time-dependent density functional theory. The DFT is used to determine the geometries and the electronic structures of the ground states. Transition energies and excited-state structures are obtained from the TDDFT calculations. Resonant energy transfer from OPV_n to MPC_{60} is also studied and the Fermi golden rule is used, along with two simple models to describe the electronic coupling to calculate the energy transfer rates. The hybrid-type PBE0 functional is used with a split-valence basis set augmented with a polarization function (SV(P)) in calculations and the calculated results are compared to the corresponding experimental results. The calculated PBE0 spectra of the OPV_n−MPC_{60} dyads correspond to the experimental spectra very well and are approximately sums of the absorption spectra of the separate OPV_n and MPC_{60} molecules. Also, the absorption energies of OPV_n and MPC_{60} and the emission energies of OPV_n are predicted well with the PBE0 functional. The PBE0 calculated resonant energy transfer rates are in a good agreement with the experimental rates and show the existence of many possible pathways for energy transfer from the first excited singlet states of the OPV_n molecules to the MPC_{60} molecule.

I. Introduction

Organic conjugated materials are of great interest for application as active components in photovoltaic devices.[1,2] Advantages of using organic materials in these devices are low cost, facile processing, thin size, and flexibility of properties and shape.[3,4] On the other hand, organic materials require a good chemical stability and large optical absorption in the visible when they are used in photovoltaic devices.[3]

During the past decade the π-conjugated polymer−fullerene systems have gained much interest as electron donor−acceptor dyads when designing organic photovoltaic cells.[5,6] A detailed understanding of the photoinduced charge transfer between a π-conjugated polymer and fullerene is required for further optimization of photovoltaic energy conversion.

Time-resolved spectroscopy has revealed that photoinduced electron transfer in poly(*p*-phenylene-vinylene)−fullerene blends occurs in the femtosecond time domain.[5,7−10] This is several orders of magnitude faster than any of the other decay processes and, therefore, the electron transfer has a high quantum efficiency.[8,10] The back-electron transfer is orders of magnitude slower than the photoinduced forward electron transfer and the charge-separated state persists, even in the microsecond and millisecond time domains, which is essential for an efficient photovoltaic device.[8]

In solar cell structures designed from fullerene-containing polymers, the electron transfer is based on processes where the locally excited state of the conjugated polymer is formed first and the electron transfer to fullerene follows. However, the experimental results[11,12] of oligo(*p*-phenylenevinylene) (OPV_n) as a donor and *N*-methylfulleropyrrolidine, synthesized by Maggini et al.[13] (MPC_{60}), as an acceptor have revealed a two-step mechanism with an ultrafast resonant energy transfer (RET) from the photoexcited conjugated chain to the covalently linked fullerene derivative, followed by a picosecond time domain hole transfer from the MPC_{60} to the OPV_n moiety. The experimental data shows that the electron transfer is much faster in films than in solutions and the RET can no longer be distinguished using the femtosecond pump−probe spectroscopy.[12]

In this paper, we use density functional theory (DFT) and time-dependent DFT (TDDFT) to study the optical transitions of the OPV_n−MPC_{60} dyads ($n = 2-4$) and of the separate OPV_n and MPC_{60} molecules. The calculated transition energies are compared to each other and to experimental values, when available. Calculations are performed using the hybrid-type PBE0 functional. The RET from OPV_n to MPC_{60} is studied by applying the Fermi golden rule with two different models—the point dipole model (PDM)[14] and the extended dipole model (EDM)[15]—to describe the electronic coupling. The experimentally observed fast RET is explained based on the calculated results. The understanding of the RET and its importance as a step preceding the electron transfer is of great interest for the ability to control the energy flow in organic materials, which strongly impacts the efficiency of an organic device. In addition, by studying the energy transfer from oligomers with a varying number of monomers, information on the effect of the chain length and an estimation for more complex chains are obtained.

The success of DFT and TDDFT in predicting the RET rates is also compared to corresponding semiempirical results obtained by Hukka et al.,[16] who used semiempirical AM1 and INDO/SCI methods to study the RET in oligo(*p*-phenylenevinylene)−fullerene dyads. They showed that it is essential to go beyond

* Author to whom correspondence should be addressed. Fax: +358.3.3115.2108. E-mail address: teemu.toivonen@tut.fi.

10.1021/jp068413v CCC: $37.00
Published on Web 05/04/2007

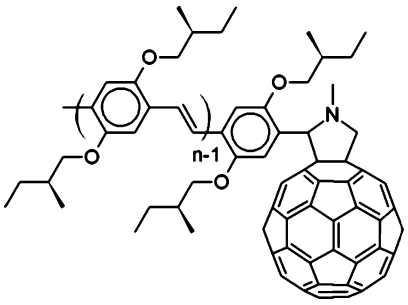

Figure 1. Molecular structure of OPV_n-MPC_{60} ($n = 2-4$).

TABLE 1. Energies (ϵ) of HOMO, LUMO, and the HOMO−LUMO Gap of OPV_n, MPC_{60}, and OPV_n-MPC_{60} Molecules, Calculated with the PBE0 Functional

molecule	ϵ_{HOMO} (eV)	ϵ_{LUMO} (eV)	ϵ_{gap} (eV)
OPV_2-MPC_{60}	−5.26	−3.37	1.89
OPV_3-MPC_{60}	−4.97	−3.38	1.59
OPV_4-MPC_{60}	−4.82	−3.37	1.45
OPV_2	−5.13	−1.26	3.87
OPV_3	−4.88	−1.69	3.19
OPV_4	−4.75	−1.88	2.87
MPC_{60}	−6.25	−3.49	2.76

the Förster model to obtain reliable estimates of the electron couplings mediating the energy-hopping process in these dyads.[16]

II. Theoretical Background and Methodology

The molecular structure of the studied oligo(*p*-phenylenevinylene)−*N*-methylfulleropyrrolidine (OPV_n-MPC_{60}, $n = 2-4$) is presented in Figure 1. First, the ground-state geometries and the electronic structures of the OPV_n-MPC_{60} dyads and of the separate OPV_n and MPC_{60} molecules were optimized using DFT.[17−20] Next, TDDFT[20,21] was used to calculate the electronic transition energies of these molecules. To obtain the fluorescence energies, the excited-state geometries of the OPV_n units were optimized using TDDFT and the electronic transition energies were calculated using these geometries.

Calculations were performed by the hybrid-type Perdew−Burke−Ernzerhof exchange correlation functional (PBE0),[22−26] in which the exchange functional is combined with the exact exchange functional from the Hartree−Fock theory (in a ratio of 25%). This functional was chosen because a previous computational study that was made by Pogantsch et al.[27] shows that the hybrid-type PBE gives singlet transition energies for oligo(*p*-phenylenevinylenes) closest to the experimental values when compared to the hybrid-type B3LYP and the local density approximation (LDA) SVWN functionals. The significancy of the exact exchange functional included from the Hartree−Fock theory was determined by comparing the results given by the generalized gradient approximation-type exchange correlation functional (PBE)[22−25] and PBE0. The PBE0 functional is shown to describe the experimental transition energies of the studied systems with much better accuracy than the PBE functional and, therefore, only the PBE0 results are presented in this article. The PBE results are presented in the Supporting Information.

In TDDFT, the electronic excitations are calculated by starting from the ground-state Kohn−Sham (KS) orbitals and their eigenvalues.[20] Thereafter, the electronic excitations are defined by means of the linear-response theory and using the adiabatic local density approximation (ALDA) for the functional derivatives of the exchange-correlation potential.[20] Only singlet states have been considered. The Karlsruhe split-valence basis sets[28,29] augmented with a polarization function (SV(P))[30] were used in all calculations. The SV(P) basis set consists of one basis function for H (4s)/[2s] and six basis functions for C, N, and O (7s4p1d)/[3s2p1d]. All DFT and TDDFT calculations have been performed using the TURBOMOLE 5.8 software package.[31,32]

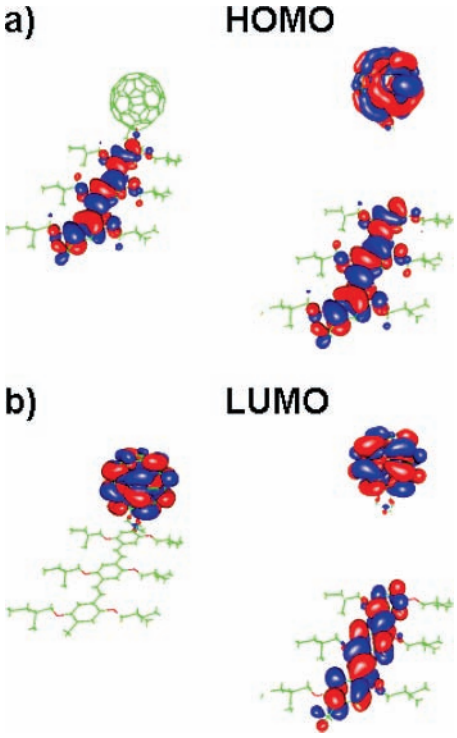

Figure 2. (a) Highest occupied molecular orbital (HOMO) and (b) lowest unoccupied molecular orbital (LUMO) yielded by the PBE0 functional for OPV_3-MPC_{60}, OPV_3, and MPC_{60}. The isoamplitude surfaces of the orbitals presented are 10% of the maximum positive (red color) and minimum negative (blue color) values of the wavefunctions.

III. Results and Discussion

Ground-State Electronic Structures of OPV_n-MPC_{60}, OPV_n, and MPC_{60}. The calculated energies of the highest occupied molecular orbital (HOMO) and the lowest unoccupied molecular orbital (LUMO) energies and the HOMO−LUMO gaps of the OPV_n, MPC_{60}, and the OPV_n-MPC_{60} dyad molecules are presented in Table 1. These results indicate that the energy of HOMO of OPV_n-MPC_{60} increases and the energy of LUMO of OPV_n-MPC_{60} remains the same when the chain length of OPV_n (i.e., the number of the PV monomers) increases.

Comparing these values to the HOMO and LUMO energies of the separate OPV_n and MPC_{60} molecules easily shows that the energy of HOMO of OPV_n-MPC_{60} corresponds to the energy of HOMO of the separate OPV_n molecule and the energy of LUMO of OPV_n-MPC_{60} corresponds to the energy of LUMO of the separate MPC_{60} molecule. There are also other OPV_n-MPC_{60} orbitals that have approximately the same energies as either an OPV_n or MPC_{60} orbital.

This means that the electronic structure of the OPV_n-MPC_{60} dyad is approximately obtained by adding together the electronic structures of the separate OPV_n and MPC_{60} molecules, as is also observed from Figure 2 where these orbitals are presented for the OPV_3-MPC_{60} dyad and its separate counterparts (the same is true for the other OPV_n-MPC_{60} dyads). As shown in Figure 2, the HOMO is delocalized over the entire *p*-phenylenevinylene chain of OPV_n, because of the delocalization of the π-electrons.

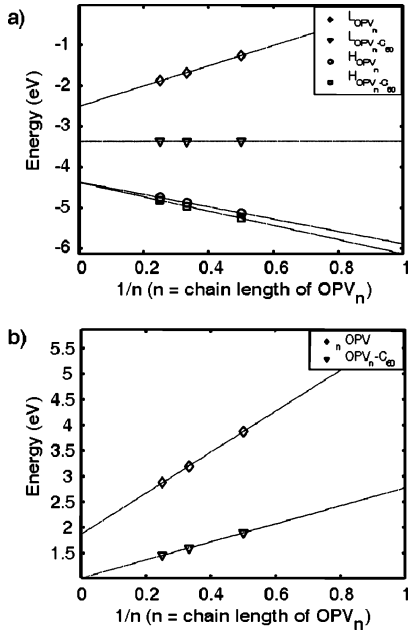

Figure 3. Energies (in electron volts) of (a) HOMOs and LUMOs, and (b) HOMO−LUMO gaps of OPV_n and OPV_n−MPC_{60} ($n = 2-4$) molecules at their ground-state structures calculated with the PBE0 functional. The lines are the best linear fits to the orbital energies.

A small interaction between OPV_n and MPC_{60} can be observed when the orbital energies of OPV_n−MPC_{60} are compared to the orbital energies of the separate molecules, i.e., the energies of HOMO and LUMO of OPV_n−MPC_{60} are ∼0.1 eV smaller and larger, respectively, than the corresponding orbital energies of the separate molecules.

The HOMO−LUMO gaps of OPV_2, OPV_3, and OPV_4 are 3.87, 3.19, and 2.87 eV, respectively. There is a clear dependence between the HOMO−LUMO gap energy and the OPV chain length; in other words, the gap energy decreases almost linearly as the chain length increases. This linear dependence of the HOMO−LUMO gap energy is presented in Figure 3 as the inverse of the number of the PV monomers, together with the energies of HOMO and LUMO. Linear dependence is also observed between the HOMO and LUMO energies and the inverse of the chain length (see Figure 3). The HOMO−LUMO gap energy of MPC_{60} is 2.76 eV, which is smaller than any of the OPV_n gap energies. Therefore, when the excited state of OPV_n is relaxed to its ground state, the energy liberated is higher than the gap energy of MPC_{60} and, therefore, an energy transfer from OPV_n to MPC_{60} is expectable.

Geometrical Structures of the OPV_n Molecules at the Ground and Excited States and the Reorganization Energies. A reorganization energy λ describes the energy change of the molecule undergoing a structural change during an electronic transition when the molecule relaxes to its potential energy minimum of the new state. The larger the reorganization energy, the more the initial and final geometries differ. There are two reorganization energies for each OPV_n, related to the transitions $S_0 \rightarrow S_1$ and $S_1 \rightarrow S_0$, which are presented in Figure 4. The first one ($\lambda_{0\rightarrow1}$) is related to the relaxation of an excited OPV_n (i.e., OPV_n*) to its excited-state potential energy minimum. The second one ($\lambda_{1\rightarrow0}$) is related to the relaxation of the OPV_n after emission to its potential energy minimum at the ground state. These reorganization energies can be determined from the energies of the minima of the ground and excited states and the transition energies. Because, in this study, the reorganization energies are calculated for molecules under vacuum at a temperature of 0 K, the values describe only the internal

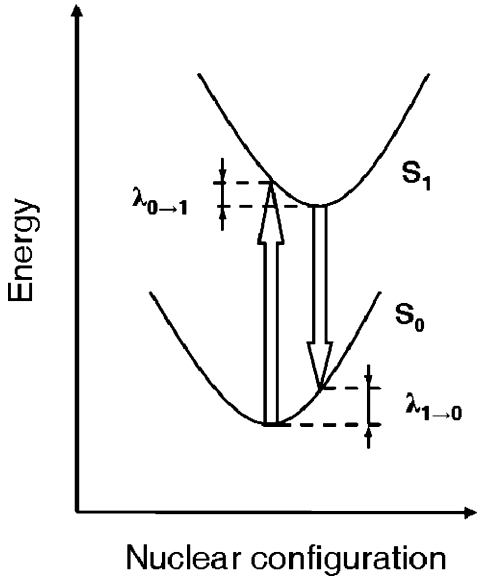

Figure 4. Definitions of the reorganization energies $\lambda_{0\rightarrow1}$ and $\lambda_{1\rightarrow0}$.

reorganization energies (i.e., the effect of solvent is not taken into account). The $\lambda_{0\rightarrow1}$ values are 0.18, 0.16, and 0.15 eV for OPV_2, OPV_3, and OPV_4, respectively, and the $\lambda_{1\rightarrow0}$ values are 0.18, 0.15, and 0.14 eV for OPV_2, OPV_3, and OPV_4, respectively. Because the reorganization energies are nonzero, the nuclear coordinates of the OPV_n molecules, i.e., the ground-state and excited-state structures of OPV_n differ from each other. The main structural differences are analyzed below. The difference between $\lambda_{0\rightarrow1}$ and $\lambda_{1\rightarrow0}$ describes the differences in the "steepnesses" of the ground-state and excited-state potential energy surfaces (molecular structures), which are very similar for all OPV_n molecules. The sum of $\lambda_{0\rightarrow1}$ and $\lambda_{1\rightarrow0}$ describes the energy difference between the absorption and emission energies between the states at issue.

The length of the double bond of vinylene in both the separate OPV_n and OPV_n of OPV_n−MPC_{60} is 1.35 Å. The single-bond length of vinylene of the corresponding structures is 1.45−1.46 Å. The C⋯C bond lengths of phenylene are 1.39−1.42 Å at the ground state. At the excited state, the double bonds of vinylene are longer by 0.02−0.05 Å and the single bonds are shorter by 0.02−0.04 Å. At the excited state, the C⋯C bond lengths of phenylene changed −0.01−0.03 Å. The ethylbutoxyl side chains are tilted slightly, compared to their ground-state structures.

Optical Transitions of OPV_n and MPC_{60}. The calculated $S_0 \rightarrow S_1$ absorption and $S_1 \rightarrow S_0$ emission energies of the OPV_n molecules and the corresponding experimental values are presented in Table 2. All $S_0 \rightarrow S_1$ transitions consist of one-electron transitions mainly (∼90% or more) from HOMO to LUMO. The TDDFT results show a bathochromic shift both in the $S_0 \rightarrow S_1$ absorption and in the $S_1 \rightarrow S_0$ emission as the number of the repeating OPV monomers increases. The $S_0 \rightarrow S_1$ transition energies are 3.36, 2.76, and 2.44 eV for OPV_2, OPV_3, and OPV_4, respectively. These results are in a good agreement with the experimental values which are 3.47, 3.05, and 2.84 eV for OPV_2, OPV_3, and OPV_4, respectively, in chloroform at room temperature.[33] The longer the OPV_n chain, the more the calculated transition energies differ from the corresponding experimental values. The $S_1 \rightarrow S_0$ transition energies are 3.00, 2.45, and 2.15 eV for OPV_2, OPV_3, and OPV_4, respectively. These results are in a very good agreement with the experimental values, which are 3.03, 2.66, and 2.47 eV for OPV_2, OPV_3, and OPV_4, respectively, in chloroform at room

TABLE 2. Absorption and the Fluorescence Energies, and the Oscillator Strengths of OPV_n and MPC_{60}, Calculated Using the TDDFT/PBE0, and the Corresponding Experimental Values

	$S_0 \rightarrow S_1$			$S_1 \rightarrow S_0$		
	calculated			calculated		
molecule	transition energy	oscillator strength	experiment	transition energy	oscillator strength	experiment
OPV_2	3.36	0.72	3.47[a]	3.00	0.80	3.03[a]
OPV_3	2.76	1.56	3.05[a]	2.45	1.71	2.66[a]
OPV_4	2.44	2.34	2.84[a]	2.15	2.55	2.47[a]
MPC_{60}	1.95	0.002	[b]			

[a] Experimental values are obtained in chloroform, from ref 33. [b] See experimental spectra in refs 13 and 38.

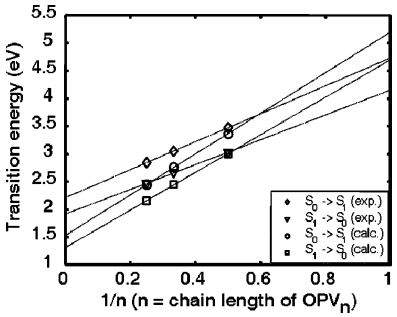

Figure 5. TDDFT/PBE0 calculated and the experimental OPV_n ($n = 2-4$) $S_0 \rightarrow S_1$ absorption and $S_1 \rightarrow S_0$ emission energies, as a function of the inverse of the chain length (n) of the OPV_n. The lines are the best linear fits to the transition energies.

temperature.[33] In the case of absorption and also in the case of fluorescence, the energy decreases when the chain length increases.

The dependence of the $S_0 \rightarrow S_1$ and $S_1 \rightarrow S_0$ transition energies on the chain length of OPV_n is illustrated in Figure 5. There is a clear linear dependence between the transition energy and the inverse of the OPV_n chain length, and this linear dependence of the transition energies on the inverse of the chain length has been established earlier experimentally as well as theoretically.[27,33-35] TDDFT results do not predict the dependence of the transition energy on the OPV_n chain length totally correctly. This is attributed to the use of ALDA for the functional derivatives of the exchange-correlation potential but not to the optimization of the geometry.[27] ALDA underestimates the excitation energies in the case of π-conjugated oligomers.[36,37] We also calculated the transition energies for the PBE-optimized OPV_n structures, using the PBE0 functional. These results differ from the PBE0 results only by $\sim$0.1 eV, meaning that the weakness of the PBE functional to predict the transition energies is mainly due to the inability to predict transition energies, not due to the inability of the PBE to predict structures.

The calculated MPC_{60} absorption spectrum shows peaks at 1.8, 2.8, and 3.3 eV and shoulders at 2.4−2.5 eV and at 3.8 eV (see Figure 6). The overall shape, as well as the characteristic energies, correspond to the experimental values[13,38] extremely well. At this point, for the energy transfer calculations presented later, it is worth noticing that the large amount of transitions in a wide energy range forming absorption of MPC_{60}. The absorption spectra simulated in the range of 1−4 eV for OPV_n and MPC_{60} are presented in Figure 6. In the spectra, the transition energies and the corresponding oscillator strengths are plotted using a Gaussian distribution function with a standard deviation of 0.10 eV.

Absorption Spectra of OPV_n−MPC_{60}. As noted previously, the electronic structure of OPV_n−MPC_{60} is approximately obtained by adding the electronic structures of the separate OPV_n and MPC_{60} molecules together and no significant interaction

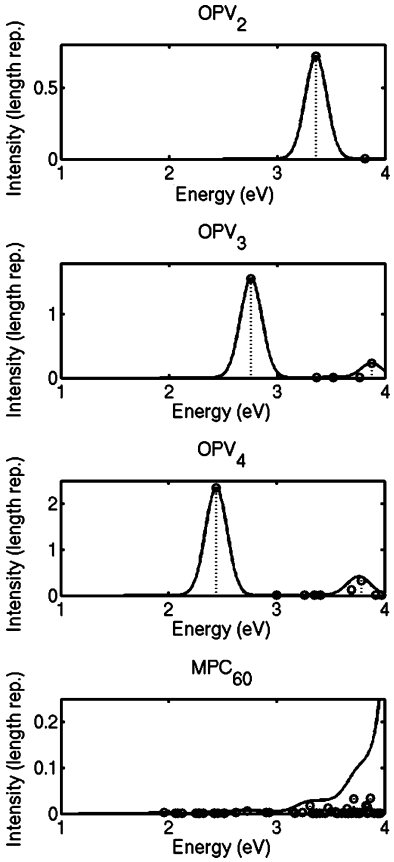

Figure 6. Absorption spectra of OPV_n ($n = 2-4$) and MPC_{60} calculated using the TDDFT/PBE0. Circles present the calculated transition energies and oscillator strengths of different transitions.

between OPV_n and MPC_{60} exists. Therefore, the absorption spectrum of OPV_n−MPC_{60} should be similar to the spectrum formed by adding the spectra of OPV_n and MPC_{60} together. The calculated spectra are presented in Figure 7. Unfortunately, because of the high computational cost of the absorption energy calculations of OPV_n−MPC_{60}, only the absorption energies up to $\sim$3.2−4.0 eV were achieved within the available computational time. Fortunately, these energies are high enough to allow a comparison with some of the lowest excited states of MPC_{60} and OPV_n. Based on the calculated results, one can make a conclusion that the absorption spectra of OPV_n−MPC_{60} are approximate sums of the absorption spectra of OPV_n and MPC_{60}, as expected. The absorption spectra of OPV_n−MPC_{60} are red-shifted by $\sim$0.1 eV, compared to the sum spectra of OPV_n and MPC_{60}, which is due to small interactions between OPV_n and MPC_{60}, as discussed previously. The similarity of the shapes of the OPV_n−MPC_{60} spectra and the sum spectra of OPV_n and MPC_{60} is also observed in the experimental spectra.[38] TDDFT shows that there is interaction between the OPV_n and C_{60} molecules at the ground state, because, in the absorption spectra

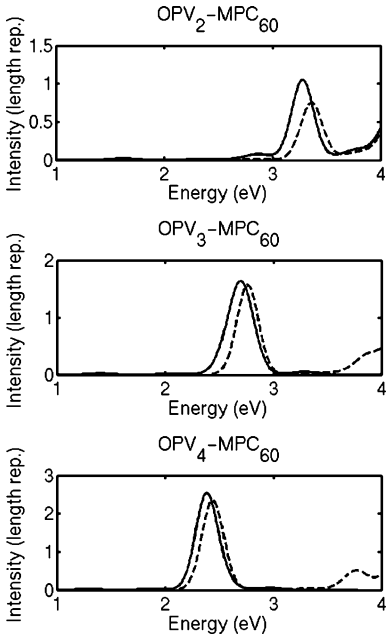

Figure 7. (—) Absorption spectra of OPV_n−MPC_{60} ($n = 2-4$) and (− − −) the sum spectra of OPV_n ($n = 2-4$) and MPC_{60} simulated on the basis of the transition energies of different transitions calculated using the TDDFT/PBE0.

of OPV_n−MPC_{60}, there are extra transitions at energies of ∼1.3−1.7 eV if compared to the sum spectra of OPV_n and MPC_{60}. In these transitions, charge is transferred from the OPV_n molecule to the MPC_{60} molecule and charge transfer states are formed. It is well-known that TDDFT does not predict excitation energies of charge-transfer excited states perfectly. This is due to the failure of exchange-correlation potentials to decay faster than the correct $1/r$ asymptotic decay, where r is the electron−nuclear distance.[39−41] These types of excited-state transitions are not discussed in the context of the experimental results. That might be due to the low energies and the low absorbances of these transitions, which make them difficult or even impossible to observe in the UV−vis spectra.

Theory and Results of the Resonant Energy Transfer Rate Calculations. To calculate the RET from the excited OPV_n (OPV_n*) to MPC_{60}, the structures of the OPV_n*−MPC_{60} systems were built by replacing OPV_n with the OPV_n* excited-state geometry in the OPV_n−MPC_{60} ground-state structure. In the weak coupling regime, RET occurs from a geometrically fully relaxed donor.[16] The RET is supposed to happen intramolecularly from the locally excited donor (OPV_n*) to MPC_{60}, so charge-transfer transitions are not considered.

On the basis of the excited-state fluorescence and the ground-state absorption properties provided by TDDFT, the total rate for the RET from an oligo(*p*-phenylenevinylene) to the fullerene derivative was calculated by summing the hopping rates over all acceptor states:

$$k_{\mathrm{RET}} = \sum_{j_A} k_{i_D - j_A} \tag{1}$$

where i_D denotes the lowest donor excited state (of OPV_n) that is involved in the donor emission and j_A runs over all acceptor excited states (of MPC_{60}) located within a 1−4 eV span from the ground state (such a large spectral range grasps all acceptor states with a significant spectral overlap with the donor emission and ensures a full convergence of the results). Each term in the summation corresponds to a pathway for energy migration and contributes to a partial rate given by eq 2 (the Fermi golden rule) in the weak coupling approximation:[42]

$$k_{i_D - j_A} = \frac{2\pi}{\hbar} V^2_{i_D - j_A} J_{i_D - j_A} \tag{2}$$

The traditional method for calculating the electronic coupling term, $V_{i_D - j_A}$, was developed by Förster (the point dipole model (PDM))[14] and is presented as

$$V_{i_D - j_A} = \frac{\kappa_{i_D - j_A} |\mu_{i_D}||\mu_{j_A}|}{4\pi\epsilon_0 R^3_{D-A}} \tag{3}$$

where $|\mu_{i_D}|$ and $|\mu_{j_A}|$ are the magnitudes of the transition dipoles of the donor and the acceptor and R_{D-A} is the distance between the centers of the chromophores. The term $\kappa_{i_D - j_A}$ is the orientation factor between the transition dipoles and is defined as

$$\kappa_{i_D - j_A} = \vec{\mu}_{i_D} \cdot \vec{\mu}_{j_A} - 3(\vec{\mu}_{i_D} \cdot \vec{R}_{D-A})(\vec{\mu}_{j_A} \cdot \vec{R}_{D-A}) \tag{4}$$

The Förster's PDM is known to fail in producing accurate couplings when the distance between the chromophores is short, compared to their planar dimensions,[43] as is the case in this study. This was also observed experimentally for OPV_4−MPC_{60} in a toluene solution[11] as well as with semiempirical methods.[16] Therefore, different models have been developed to describe the electronic coupling between molecules with a short intermolecular distance and for taking into account the three-dimensional structure of the transition density. Other models include, for example, the extended dipole model (EDM)[15] and atomic transition density model (ATDM),[16,42] as well as the transition density cube method,[44] which take the chemical structure and the topology of the interacting chromophores into account and thereby produce more-reliable couplings. Because the transition densities are not available from the current version of the software used, the EDM is used in addition to PDM to define the electronic couplings between the interacting chromophores of the studied molecules.

In the extended dipole model, the donor (acceptor) is replaced by the dipoles of the two opposite charges $+q_{i_D}$ ($+q_{j_A}$) and $-q_{i_D}$ ($-q_{j_A}$) at a distance of $|\vec{l}_{i_D}|$ ($|\vec{l}_{j_A}|$). The dipole is assumed to have a value and a direction of the transition moment $\vec{\mu}_{i_D}$ ($\vec{\mu}_{j_A}$), i.e.,

$$\vec{\mu}_{i_D} = q_{i_D} \vec{l}_{i_D} \tag{5a}$$

and

$$\vec{\mu}_{j_A} = q_{j_A} \vec{l}_{j_A} \tag{5b}$$

The $|\vec{l}_{i_D}|$ and $|\vec{l}_{j_A}|$ are generally chosen to be on the order of the size of the chromophores. In the case of OPV_n, distances between the center points of the outermost phenyl rings, i.e., 6.6, 13.2, and 19.8 Å, were chosen for the l_D values for OPV_2, OPV_3, and OPV_4, respectively. The l_A value of MPC_{60} is 7.3 Å, which corresponds approximately to the diameter of the C_{60} fragment, because the transition densities of MPC_{60} are mainly located on C_{60}.[16]

The electronic coupling term, $V_{i_D - j_A}$ (expressed in units of cm^{-1}), for different channels in eq 2, according to the EDM, is defined as follows:

$$V_{i_D - j_A} = \frac{q_{i_D} q_{j_A}}{4\pi\epsilon_0}\left(\frac{1}{a_{1,i_D - j_A}} + \frac{1}{a_{2,i_D - j_A}} - \frac{1}{a_{3,i_D - j_A}} - \frac{1}{a_{4,i_D - j_A}}\right) \tag{6}$$

where q_{i_D} (q_{j_A}) is the charge of the donor (acceptor) obtained

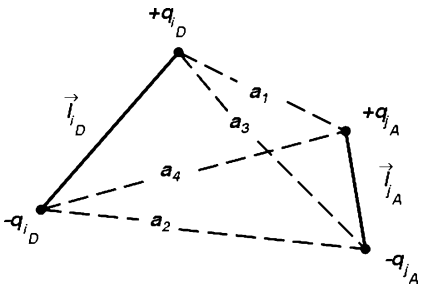

Figure 8. Definition of the parameters of the two dipoles used to calculate the electronic couplings.

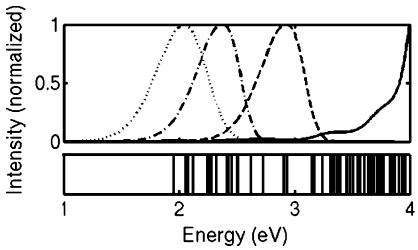

Figure 9. (− − −) Normalized emission spectra of OPV_2, (− · −) OPV_3, and (· · ·) OPV_4, and (—) the absorption spectrum of MPC_{60} simulated on the basis of the excitation energies of different transitions calculated by using the TDDFT/PBE0. The vertical lines describe the transition energies of MPC_{60}.

from formula[3] for the excited state *i* (*j*). Distances a_{k,i_D-j_A} (k = 1, 2, 3, 4) represent the distances between the charges $\pm q_{i_D}$ ($\pm q_{j_A}$) and are presented in Figure 8. The orientation of the distance $\vec{l}_{i_D}$ ($\vec{l}_{j_A}$)was set to be the same as the orientation of the transition dipole moment $\vec{\mu}_{i_D}$ ($\vec{\mu}_{j_A}$).

The EDM is known to be a good approximation for strongly allowed transitions for molecules where the separation of chromophores is small, compared to their planar dimensions, and less good for weakly allowed transitions.[45] The EDM has been originally used to describe an electronic coupling of dye molecules in aggregates;[15] however, in this study, it is applied to defining coupling between two molecules of different types. For all OPV_n molecules, the $S_1 \rightarrow S_0$ transition is strongly allowed (the transition dipole moments are ∼10 D); however, for MPC_{60}, most of the $S_0 \rightarrow S_n$ transitions are weakly allowed (the transition dipole moments are <1 D). For this reason, the energy transfer is taking place between strongly and weakly allowed transitions, in addition to strongly and strongly allowed transitions. From the calculated RET rates, which are presented later, it can be observed that EDM predicts the experimental rates better than PDM. The rates obtained with TDDFT/EDM are on the same order of magnitude as the semiempirical/ATDM results.[16] Therefore, EDM seems to work well for the electronic coupling calculations, at least in the case of these molecules in which strongly allowed transitions also are mixed with the weakly allowed transitions and not only with the strongly allowed transitions.

A displaced harmonic oscillator model was applied to compute the normalized absorption and emission spectra and the spectral overlap factors (*J*) in eq 2 numerically:[46,47]

$$J_{i_D-j_A} = \int_0^\infty \mathrm{d}E\, F_{i_D}(E) A_{j_A}(E) \tag{7}$$

where $F_{i_D}(E)$ and $A_{j_A}(E)$ denote the donor emission and the acceptor absorption spectra, respectively, normalized on a cm^{-1} scale.

The spectral intensity was approximated by the superposition of transitions between vibrational manifolds of the ground states and electronically excited states. In a hypothetical case of displacing the quadratic potential energy surfaces along one single normal mode, the probability for the $0-\nu$ vibrational transition at 0 K is given by the square of the vibronic coupling term, i.e., the Franck−Condon factor (FCF):[48]

$$\mathrm{FCF}_{0-v} = \frac{e^{-S}S^v}{v!} \tag{8}$$

where *S* is the Huang−Rhys factor, which is expressed in terms of the reorganization energy (λ) and the vibrational energy of the effective mode ($\hbar\langle\omega\rangle$):

$$S = \frac{\lambda}{\hbar\langle\omega\rangle} \tag{9}$$

For the OPV_n segment, a simple one-mode vibronic approach was applied. The Huang−Rhys factor of $S = 0.9$ and the effective vibrational energy of $\hbar\langle\omega\rangle = 0.17$ eV were selected for all OPV_n molecules. This vibrational frequency corresponds to the experimentally observed C═C stretching vibrational frequency of oligo(*p*-phenylvinylenes).[33] The measured optical absorption spectra of fullerene derivatives do not show any fine structure, which might be related to the overlap between many closely lying weak bands, leading to rather broad and featureless spectra of fullerene derivatives.[11,13,38] Thus, only the energies of the vertical transitions were used in the simulation of the acceptor absorption, with no attempt to account for the coupling to vibrations. Emission and absorption spectra were convoluted with Gaussian functions with a 0.10 eV standard deviation, which yields, together with the other parameters, spectral shapes in close agreement with the experimental results. The simulated OPV_n (n = 2−4) photoluminescence spectra and the MPC_{60} absorption spectrum are shown in Figure 9. The shape of the simulated absorption spectrum of MPC_{60} shows absorption over the entire visible spectral range, and the main features are located at 1.8, 2.4−2.5, 2.8, 3.3, and 3.8 eV, as discussed previously. The calculated transition energies of MPC_{60} are shown as vertical lines under the spectra. The connection of the main features of the MPC_{60} absorption spectrum to RET is explained later.

The calculated and measured RET rates of OPV_n−MPC_{60} are presented in Table 3. The TDDFT/PBE0 calculated k_{RET} values are 1.5, 0.7, and 0.2 ps^{-1} for OPV_2−MPC_{60}, OPV_3−MPC_{60}, and OPV_4−MPC_{60}, respectively. The calculated rates are ∼2−5 times smaller than the corresponding experimental rates when the EDM is used, and the decrease in the k_{RET} value is predicted very well when the OPV_n chain length is increased. The RET rates obtained using the semiempirical method and the atomic transition density model[16] are in a slightly closer agreement with the experimental rates than with the TDDFT/PBE0 rates. The rates calculated with the PDM from the TDDFT results differ significantly from the experimental values. This was previously seen also with the semiempirical method.[16] The OPV_4−MPC_{60} rate especially is an order of magnitude smaller than the corresponding experimental value. Because the EDM RET rates agree with experimental values better than PDM, only EDM results are analyzed in more detail below.

Table 4 shows the MPC_{60} acceptor states that have the dominant contributions to the total RET rate as well as with the corresponding electronic couplings ($V_{i_D-j_A}$) and the spectral-overlap factors($J_{i_D-j_A}$). A large contribution to the total RET rate requires significant $V_{i_D-j_A}$ and $J_{i_D-j_A}$ values, as can be seen from eq 2. The largest contributions result from the excited states of MPC_{60} at energies of ∼2.3−2.5 eV and at 2.8−2.9 eV. These

TABLE 3. Resonant Energy Transfer Rate Constants of the OPV_n−MPC_{60} Dyads Calculated Using the TDDFT/PBE0 and the Extended Dipole Model Results, as well as the Semiempirical Method and the Atomic Transition Density Model Results, and also the Corresponding Experimental Values[a]

	Resonant Energy Transfer Rate Constant, k_{RET} ($\times 10^{12}$ s^{-1})				
	calculated				
	TDDFT/PBE0		SE[b]		
dyad	extended dipole model, EDM	point dipole model, PDM	atomic transition density model, ATDM	point dipole model, PDM	experimental[c]
OPV_2−MPC_{60}	1.5	1.0	6.6	1.1	2.9
OPV_3−MPC_{60}	0.7	0.3	2.3	0.3	2.1
OPV_4−MPC_{60}	0.2	0.1	0.5	0.1	1.1

[a] The point dipole model results are also given. [b] Semiempirical values are taken from ref 16. [c] Experimental values are obtained in toluene (taken from ref 38).

TABLE 4. Contributions $k_{i_D-j_A}$ to the Total Energy Transfer Rates (k_{RET}) from the Dominant Pathways Associated with MPC_{60} Acceptor States (j_A) Calculated Using the TDDFT/PBE0 and the Extended Dipole Model Results[a]

MPC_{60} excited state, j_A	transition energy (eV)	$k_{i_D-j_A}$ ($\times 10^{12}$ s^{-1})	$V_{i_D-j_A}$ (cm^{-1})	$J_{i_D-j_A}$ ($\times 10^{-3}$ cm)
		OPV_2−MPC_{60} Dyad		
S_{10}	2.42	0.08	46	0.03
S_{11}	2.45	0.04	27	0.04
S_{16}	2.83	0.28	32	0.22
S_{17}	2.86	1.04	62	0.23
S_{19}	3.17	0.02	13	0.08
		OPV_3−MPC_{60} Dyad		
S_6	2.27	0.03	11	0.22
S_9	2.39	0.03	11	0.23
S_{10}	2.42	0.42	40	0.23
S_{11}	2.45	0.15	25	0.21
S_{12}	2.51	0.03	12	0.17
		OPV_4−MPC_{60} Dyad		
S_1	1.95	0.02	11	0.18
S_6	2.27	0.02	11	0.12
S_9	2.39	0.01	11	0.06
S_{10}	2.42	0.08	36	0.05
S_{11}	2.45	0.02	21	0.04

[a] Transition energies, electronic couplings ($V_{i_D-j_A}$), and the spectral overlap factors ($J_{i_D-j_A}$) are also indicated for each channel.

correspond to the shoulder and the peak of the absorption spectrum of MPC_{60}, as previously discussed. Also, the "excited-state density" is high at these energies and especially at energies of >3.0 eV. The emission spectrum of OPV_2 overlaps with a widest range of the excited states of MPC_{60}, whereas the emission spectra of OPV_3 and OPV_4 overlap with much fewer MPC_{60} excited states, as seen in Figure 9. This means that there are more possible energy-transfer channels from OPV_2 than from OPV_3 or OPV_4 to MPC_{60}. Together with the electronic couplings, this also effects the energy-transfer rate and makes it the fastest for OPV_2−MPC_{60}. Overall, the energy transferred from an excited OPV_n molecule can excite the MPC_{60} to many different excited states, inducing a fast RET.

IV. Conclusions

We have studied the ability of density functional theory (DFT) and time-dependent density functional theory (TDDFT) to predict the optical transitions of the OPV_n−MPC_{60} ($n = 2-4$) dyad and the separate OPV_n and MPC_{60} molecules with the hybrid type PBE0 functional. The calculated $S_0 \rightarrow S_1$ transition energies of OPV_n are only 0.1−0.4 eV smaller than the experimental energies. The calculated energies of the first excited-state emissions of different OPV_n are in good agreement with the experimental values, although all calculations predict a stronger bathocromic shift for OPV_n fluorescence than found in the experiments. For the $S_1 \rightarrow S_0$ transition, the calculated energies are 0−0.3 eV smaller than the experimental energies. The longer the OPV_n chain length, the more the calculated transition energies differ from the experimental values. The calculations predict the overall shape and the characteristic energies of the MPC_{60} absorption spectrum very well. The calculated absorption spectra of OPV_n−MPC_{60} are observed to be approximately the sums of the absorption spectra of the separate OPV_n and MPC_{60} molecules, as is the case with the experimental spectra. Calculations reveal a low-intensity band near the infrared region, which is attributed to a charge-transfer state that is not seen in the experiments.

We have also used the extended dipole model (EDM) together with the results of the TDDFT description of the electronic excitations to study the resonant energy transfer (RET) in the OPV_n−MPC_{60} dyads. The RET rates calculated from the TDDFT/PBE0 transitions using the EDM are comparable to the experimental values, taking into account the crudeness of the EDM used. The calculated k_{RET} values are 1.5, 0.7, and 0.2 ps^{-1} for OPV_2−MPC_{60}, OPV_3−MPC_{60}, and OPV_4−MPC_{60}, respectively. The fast RET rates observed for OPV_n−MPC_{60} molecules can be explained by the high number of possible MPC_{60} excited states absorbing the energy from the excited OPV_n. The amount of absorbing states of MPC_{60} that overlap with the emission spectra of OPV_n is the highest for OPV_2, whereas the emission spectra of OPV_3 and OPV_4 overlap with much fewer of the MPC_{60} excited states. Therefore, more possible energy-transfer channels exist from OPV_2 than from OPV_3 or OPV_4 to MPC_{60}, and, together with the electronic couplings, this causes the energy-transfer rate to be the fastest for OPV_2−MPC_{60}.

Acknowledgment. The authors acknowledge helpful discussions with Dr. D. Beljonne (University of Mons-Hainaut and Georgia Institute of Technology), Prof. J.-L. Brédas (Georgia Institute of Technology and University of Mons-Hainaut), and Prof. T. T. Rantala (Tampere University of Technology). Prof. H. Lemmetyinen, the head of the Institute of Materials Chemistry at Tampere University of Technology, is acknowledged for offering the facilities for this research. The work is supported by the Academy of Finland. The computations presented in this document have been made with the CSC's computing environment. (CSC is the Finnish IT Center for Science and is owned by the Ministry of Education.) T.L.J.T. also thanks the Emil Aaltonen Foundation, Tampere, Finland, for a traveling allowance to visit at the Georgia Institute of Technology. T.I.H. also thanks the Georgia Institute of Technology for a research fellowship.

Supporting Information Available: Figures of spectra, tables of energies of orbitals and transitions and the reorganization energies calculated with the general gradient approximation type PBE functional (PDF). This material is available free of charge via the Internet at http://pubs.acs.org.

Note Added after ASAP Publication. This article was released ASAP on May 5, 2007. The Supporting Information has been revised and posted on May 11, 2007.

References and Notes

(1) Friend, R. H.; Gymer, R. W.; Holmes, A. B.; Burroughes, J. H.; Marks, R. N.; Taliani, C.; Bradley, D. C. C.; Dos Santos, D. A.; Brédas, J.-L.; Lögdlund, M.; Salaneck, W. R. *Nature (London)* **1999**, *397*, 121.

(2) Halls, J. J. M.; Walsh, C. A.; Greenham, N. C.; Marseglia, E. A.; Friend, R. H.; Moratti, S. C.; Holmes, A. B. *Nature* **1995**, *376*, 498.

(3) Brabec, C. J.; Sariciftci, N. S.; Hummelen, J. C. *Adv. Funct. Mater.* **2001**, *11*, 15.

(4) Burroughes, J. H.; Bradley, D. D. C.; Brown, A. R.; Marks, R. N.; Mackay, K.; Friend, R. H.; Burns, P. L.; Holmes, A. B. *Nature (London)* **1990**, *347*, 539.

(5) Sariciftci, N. S.; Smilowitz, L.; Heeger, A. J.; Wudl, F. *Science* **1992**, *258*, 1474.

(6) Yu, G.; Gao, J.; Hummelen, J. C.; Wudl, F.; Heeger, A. J. *Science* **1995**, *270*, 1789.

(7) Kraabel, B.; McBranch, D.; Sariciftci, N. S.; Heeger, A. J. *Phys. Rev. B* **1994**, *50*, 18543.

(8) Kraabel, B.; Hummelen, J. C.; Vacar, D.; Moses, D.; Sariciftci, N. S.; Heeger, A. J. *J. Chem. Phys.* **1996**, *104*, 4267.

(9) Brabec, C. J.; Zerza, G.; Cerullo, G.; De Silvesteri, S.; Luzzati, S.; Hummelen, J. C.; Sariciftci, N. S. *Chem. Phys. Lett.* **2001**, *340*, 232.

(10) Moses, D.; Dogariu, A.; Heeger, A. J. *Chem. Phys. Lett.* **2000**, *316*, 356.

(11) van Hal, P. A.; Janssen, R. A. J.; Lanzani, G.; Cerullo, G.; Zavelani-Rossi, M.; De Silvestri, S. J. *Phys. Rev. B.* **2001**, *64*, 075206.

(12) van Hal, P. A.; Meskers, S. C. J.; Janssen, R. A. J. *Appl. Phys. A* **2004**, *79*, 41.

(13) Maggini, M.; Scorrano, G. *J. Am. Chem. Soc.* **1993**, *115*, 9798.

(14) Förster, T. *Ann. Phys.* **1948**, *2*, 55.

(15) Czikklely, V.; Forsterling, H. D.; Kuhn, H. *Chem. Phys. Lett.* **1970**, *6*, 207.

(16) Hukka, T. I.; Toivonen, T.; Hennebicq, E.; Brédas, J.-L.; Janssen, R. A. J.; Beljonne, D. *Adv. Mater.* **2006**, *18*, 1301.

(17) Hohenberg, P.; Kohn, W. *Phys. Rev. B* **1964**, *136*, B864.

(18) Kohn, W.; Sham, L. *Phys. Rev. A* **1965**, *140*, A1133.

(19) Koch, W.; Holthausen, M. C. *A Chemist's Guide to Density Functional Theory*, Second Edition; Wiley−VCH: Weinheim, Germany, 2001.

(20) Seminario, J. M. *Recent Developments and Applications of Modern Density Functional Theory*; Elsevier: Amsterdam, 1996.

(21) Furche, F.; Ahlrichs, R. *J. Chem. Phys.* **2002**, *117*, 7433.

(22) Dirac, P. A. M. *Proc. R. Soc. London A* **1929**, *123*, 714.

(23) Perdew, J. P.; Wang, Y. *Phys. Rev. B* **1992**, *45*, 13244.

(24) Perdew, J. P.; Burke, K.; Ernzerhof, M. *Phys. Rev. Lett.* **1996**, *77*, 3865.

(25) Slater, J. C. *Phys. Rev.* **1951**, *81*, 385.

(26) Perdew, J. P.; Ernzerhof, M.; Burke, K. *J. Chem. Phys.* **1996**, *105*, 9982.

(27) Pogantsch, A.; Heimel, G.; Zojer, E. *J. Chem. Phys.* **2002**, *117*, 5921.

(28) Schäfer, A.; Horn, H.; Ahlrichs, R. *J. Chem. Phys.* **1992**, *97*, 2571.

(29) Schäfer, A.; Huber, C.; Ahlrichs, R. *J. Chem. Phys.* **1994**, *100*, 5829.

(30) Dunning, T. H., Jr. *J. Chem. Phys.* **1989**, *90*, 1007.

(31) Ahlrichs, R.; Bär, M.; Häser, M.; Horn, H.; Kölmel, C. *Chem. Phys. Lett.* **1989**, *162*, 165.

(32) Treutler, O.; Ahlrichs, R. *J. Chem. Phys.* **1995**, *102*, 346.

(33) Peeters, E.; Ramos, A. M.; Meskers, S. C. J.; Janssen, R. A. J. *J. Chem. Phys.* **2000**, *112*, 9445.

(34) Beljonne, D.; Shuai, Z.; Friend, R. H.; Brédas, J. L. *J. Chem. Phys.* **1995**, *102*, 2042.

(35) Cornil, J.; Beljonne, D.; Heller, C. M.; Campbell, I. H.; Laurich, B. K.; Smith, D. L.; Bradley, D. D. C.; Müllen, K.; Brédas, J. L. *Chem. Phys. Lett.* **1997**, *278*, 139.

(36) Champagne, B.; Perpète, E. A.; van Gisbergen, S. J. A.; Baerends, E.-J.; Snijders, J. G.; Soubra-Ghaoui, C.; Robins, K. A.; Kirtman, B. *J. Chem. Phys.* **1998**, *109*, 10489.

(37) van Faasen, M.; de Boeij, P. L. *J. Chem. Phys.* **2004**, *121*, 10707.

(38) Peeters, E.; van Hal, P. A.; Knol, J.; Brabec, C. J.; Sariciftci, N. S.; Hummelen, J. C.; Janssen, R. A. J. *J. Phys. Chem. B* **2000**, *104*, 10174.

(39) Dreuw, A.; Weisman, J. L.; Head-Gordon, M. *J. Chem. Phys.* **2003**, *119*, 2943.

(40) Tozer, D. J. *J. Chem. Phys.* **2003**, *119*, 12697.

(41) Dreuw, A.; Head-Gordon, M. *J. Am. Chem. Soc.* **2004**, *126*, 4007.

(42) Hennebicq, E.; Pourtois, G.; Scholes, G. D.; Herz, L. M.; Russell, D. M.; Silva, C.; Setayesh, S.; Grimsdale, A. C.; Müllen, K.; Brédas, J.-L.; Beljonne, D. *J. Am. Chem. Soc.* **2005**, *127*, 4744.

(43) Murrel, J. N.; Tanaka, J. *J. Mol. Phys.* **1964**, *7*, 364.

(44) Krueger, B. P.; Scholes, G. D.; Fleming, G. R. *J. Phys. Chem. B* **1998**, *102*, 5378.

(45) Markovitsi, D.; Germain, A.; Millié, P.; Lécuyer, P.; Gallos, L.; Argyrakis, P.; Bengs, H.; Ringsdorf, H. *J. Phys. Chem.* **1995**, *99*, 1005.

(46) Lax, M. *J. Chem. Phys.* **1952**, *20*, 1752.

(47) May, V.; Kühn, O. *Charge and Energy Transfer Dynamics in Molecular Systems*, 2nd Edition; Wiley−VCH, Weinheim, Germany, 2004.

(48) Karaburnaliev, S.; Bittner, E.; Baumgarten, M. *J. Chem. Phys.* **2001**, *114*, 5863.